LETTERS

Transparent dense sodium

Yanming Ma[1,2], Mikhail Eremets[3], Artem R. Oganov[2,4]†, Yu Xie[1], Ivan Trojan[3], Sergey Medvedev[3], Andriy O. Lyakhov[2]†, Mario Valle[5] & Vitali Prakapenka[6]

Under pressure, metals exhibit increasingly shorter interatomic distances. Intuitively, this response is expected to be accompanied by an increase in the widths of the valence and conduction bands and hence a more pronounced free-electron-like behaviour. But at the densities that can now be achieved experimentally, compression can be so substantial that core electrons overlap. This effect dramatically alters electronic properties from those typically associated with simple free-electron metals such as lithium (Li; refs 1–3) and sodium (Na; refs 4, 5), leading in turn to structurally complex phases[6–8] and superconductivity with a high critical temperature[9–11]. But the most intriguing prediction—that the seemingly simple metals Li (ref. 1) and Na (ref. 4) will transform under pressure into insulating states, owing to pairing of alkali atoms—has yet to be experimentally confirmed. Here we report experimental observations of a pressure-induced transformation of Na into an optically transparent phase at ~200 GPa (corresponding to ~5.0-fold compression). Experimental and computational data identify the new phase as a wide bandgap dielectric with a six-coordinated, highly distorted double-hexagonal close-packed structure. We attribute the emergence of this dense insulating state not to atom pairing, but to *p–d* hybridizations of valence electrons and their repulsion by core electrons into the lattice interstices. We expect that such insulating states may also form in other elements and compounds when compression is sufficiently strong that atomic cores start to overlap strongly.

Sodium adopts the body-centred cubic (b.c.c.) structure at ambient conditions. Under pressure, it transforms to the face-centred cubic (f.c.c.) structure at 65 GPa (ref. 12) and to the cI16 structure at 103 GPa (refs 7, 13). In recent experiments[7,8,13], further compression to 160 GPa yielded a number of phases in a narrow pressure–temperature range near the minimum of the melting curve (melting temperature $T_{melt} \approx 300$ K at 118 GPa). Theoretical calculations[4,14] suggest stable body-centred tetragonal (Cs-IV) and α-Ga (*Cmca*) structures for pressures above 190 GPa. The α-Ga structure is especially interesting, because the calculations suggest a zero bandgap above 800 GPa owing to pairing of Na atoms[4]. To explore the possible existence of stable yet hitherto unsuspected high-pressure structures and thus advance our understanding of the pressure-induced metal–insulator transition in Na, we undertook an extensive experimental and theoretical study into insulating states in this archetypal metal at high pressures.

Our diamond-anvil cell experiments (see Methods for details) yielded X-ray diffraction data at 101 and 113 GPa corresponding to the known f.c.c. ($a = 3.46$ Å) and cI16 phases ($a = 5.44$ Å), respectively, in agreement with available experimental data[7,12,15]. The corresponding Raman spectra show no features at pressures below 130 GPa. But a pronounced Raman spectrum appears at higher pressures (Fig. 1a), indicating a major phase transformation that according to visual observation is associated with a gradual decrease in the reflection of visible light from the sample. The Raman spectra appearing around 130 GPa are in good accordance with the theoretical spectra calculated for the experimentally observed[7,8] oP8 (*Pnma*) phase (Supplementary Fig. 1d). Above 150 GPa, the Raman spectra again show marked changes, including a strong decrease in intensity, that signify another phase transition (Fig. 1a). The X-ray diffraction pattern of this phase is consistent with the tI19 structure[7,8].

Na becomes optically transparent at pressures of ~200 GPa. (The onset of transparency occurred at 208 GPa in the run shown in Fig. 2a, and at 194 GPa in the run shown in Supplementary Fig. 1a.) The edge in the absorption spectrum (Supplementary Fig. 1c) gives for transparent Na a bandgap of at least ~1.3 eV. The onset of transparency coincides with dramatic changes in the Raman spectra (Fig. 1a), particularly the appearance of a single intense line centred at ~340 cm^{-1}. On releasing the pressure, the transparent phase persists to 182 GPa; at that point, the sample reverts to opaque and exhibits

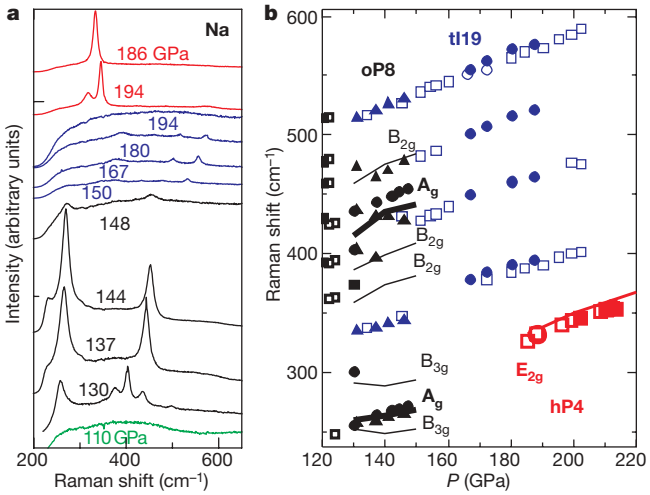

Figure 1 | Raman spectra of sodium. a, Raman spectra obtained at increasing pressures. Spectra of cI16, oP8, tI19 and transparent phases, where the intensities of different phases are representative, are shown by green, black, blue and red lines, respectively. **b**, Pressure dependence of Raman peaks for five pressure runs. The colours correspond to the spectra in **a**. Filled and open symbols correspond to runs on pressure increase and decrease, respectively. Black lines are theoretical Raman modes for the oP8 structure (thicker lines and bold font labels for intense peaks); the red line is the E_{2g} mode for transparent Na-hP4. No Raman calculations were performed for the complex tI19 phase. Phase names are also shown bold.

[1]National Laboratory of Superhard Materials, Jilin University, Changchun 130012, China. [2]Laboratory of Crystallography, Department of Materials, ETH Zurich, Wolfgang-Pauli-Str. 10, CH-8093 Zurich, Switzerland. [3]Max-Planck-Institut für Chemie, Postfach 3060, 55020 Mainz, Germany. [4]Geology Department, Moscow State University, 119992 Moscow, Russia. [5]Data Analysis and Visualization Services, Swiss National Supercomputing Centre (CSCS), Cantonale Galleria 2, 6928 Manno, Switzerland. [6]Consortium for Advanced Radiation Sources, University of Chicago, Chicago, Illinois 60637, USA. †Present address: Department of Geosciences and New York Center for Computational Science, Stony Brook University, Stony Brook, New York 11794-2100, USA.

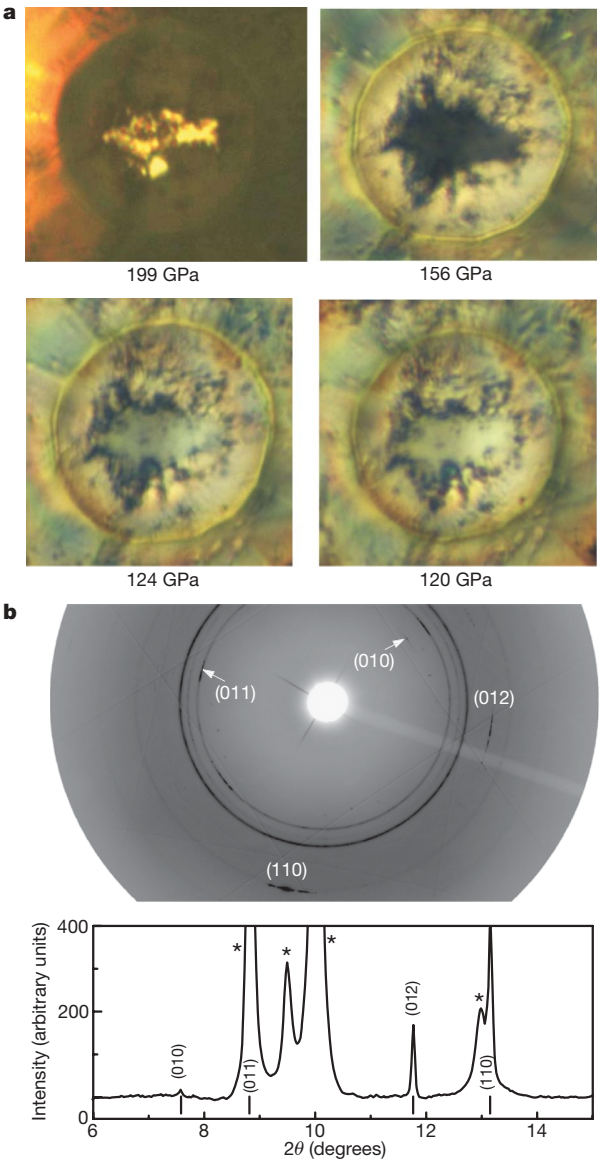

Figure 2 | Phase transformations in Na at megabar pressures. **a**, Photographs of the Na sample taken under combined transmitted and reflected illumination (see also Supplementary Fig. 1) at releasing pressure for different phases: 199 GPa (transparent phase), 156 GPa (tI19), 124 GPa (oP8) and 120 GPa (cI16). The transparent phase was created at 208 GPa, but remained when pressure was dropped to 199 GPa, similar to the outcome of another run (Supplementary Fig. 1). The diameter of the culet of the diamond anvil is 30 μm. **b**, X-ray CCD image and integrated diffraction pattern taken at 190 GPa from the transparent Na sample. Tick marks show the calculated reflection positions for Na-hP4. Asterisks indicate reflections from the Re gasket.

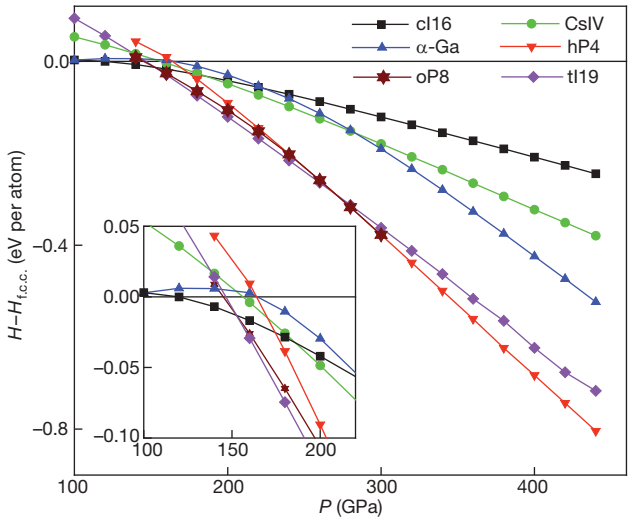

Figure 3 | Enthalpy curves (relative to f.c.c.) as a function of pressure for cI16, CsIV, α-Ga, oP8, tI19 and hP4 structures of Na. The inset shows the transition sequence f.c.c. → cI16 → tI19 (oP8) → hP4 in more detail. Two phase transitions, cI16 → tI19 → hP4, are predicted at 152 and 260 GPa, respectively. The oP8 structure is less stable than the tI19 phase in the pressure range 152–260 GPa, but is energetically very competitive. It is noteworthy that temperature effects (or lattice energies) are not considered in the calculation, but might play an important structural role. Note also that tI19 is an incommensurate structure; thus, its enthalpy calculations were performed with the periodic approximant (Supplementary Fig. 4). The continuous merging of the enthalpy curves of oP8 and hP4 at 250 GPa is due to the second-order nature of the oP8→hP4 transition (Supplementary Fig. 2).

Raman spectra typical of the tI19 phase (Fig. 1a). On further decompression, Na first transforms at 132 GPa to the oP8 phase and finally, at 120 GPa, to a highly reflective metallic state devoid of any Raman signal.

We performed extensive structure searches, which were unbiased by prior knowledge and based on global optimization using the *ab initio* evolutionary methodology for crystal structure prediction[16–19]. Our variable-cell simulations yielded below 260 GPa the experimentally known f.c.c[7,12], cI16[7,8,15] and oP8[7,8] phases (Fig. 3), though the latter is calculated to be marginally less stable than the tI19 phase (see also Fig. 3 inset). Over the pressure range of nearly equal enthalpies for oP8 and tI19, 152–260 GPa, the energy landscape of Na is overall flat yet exhibits a complex pattern of many shallow local minima; as a result, our simulated structure search identified many distinct structures having enthalpies within 30 meV per atom of the ground state. Note, however, that the experiments were carried out at room temperature, whereas the calculations assume $T = 0$ K; moreover, we neglect phonon enthalpies arising from coupling between nuclei and electrons, which can influence the stable structure of the system.

Higher-pressure simulations, at 320 and 1,000 GPa, revealed a simple but unusual structure, which can be described as a double-hexagonal close-packed (d.h.c.p.) structure squeezed along the *c*-axis (Pearson symbol hP4). The 'squeezing' results in an extremely small c/a ratio of, for example, 1.391 at 320 GPa; this ratio is less than half the ideal value of $c/a = 2(8/3)^{1/2} = 3.266$ seen in the normal d.h.c.p structure that corresponds to the densest packing of spherical particles. Atoms in this dense Na structure are six-fold coordinated (Fig. 4a). The characteristic double-well energy profile (Supplementary Fig. 8a) and the six-coordinate topology render Na-hP4 structurally, energetically and electronically distinct from normal d.h.c.p. Remarkably, the energy barrier between two minima in Na-hP4 occurs at $c/a = 3.266$, where Cs-d.h.c.p. has a stable minimum (Supplementary Fig. 8).

The electronic structure of Na-hP4 (Fig. 4b) gives rise to an intriguing insulating state characterized by a large occupancy of *d* orbitals that are involved in *p*–*d* hybridizations. GW calculations (known to provide accurate description of bandgaps, within 10% of experimental values[20]) summarized in Fig. 4d show that Na-hP4 possesses a large energy gap of 1.3 eV at 200 GPa (where the atomic volume is 7.88 Å^3 per atom), and that the gap rapidly increases with increasing pressure to reach 6.5 eV at 600 GPa (5.03 Å^3 per atom).

Although we have been unable to directly determine the structure of the transparent phase observed above pressures of about 200 GPa, the comparison of experimental and theoretical data identifies it reliably as Na-hP4. For example, the optical transparency of the dense Na sample is in agreement with the large bandgaps calculated for this phase. And although the quality of the X-ray diffraction pattern obtained for the transparent phase is insufficient to derive an exact structure solution, the observed reflections are well indexed as Na-hP4, with lattice parameters of $a = b = 2.92$ Å and $c = 4.27$ Å at

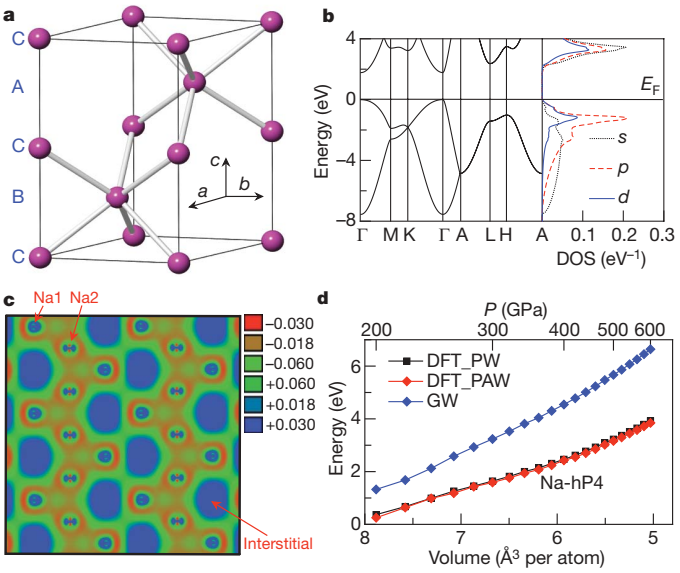

Figure 4 | Structural and electronic properties of Na-hP4. a, Crystal structure of Na-hP4 (space group $P6_3/mmc$). Lattice parameters at 320 GPa (6.50 Å^3 per atom): $a = b = 2.784$ Å and $c = 3.873$ Å. There are two inequivalent atomic positions: Na1 at 2*a* (0.0, 0.0, 0.0) and Na2 at 2*d* (2/3, 1/3, 1/4). **b**, Band structure (left panel) and partial densities of states (DOS; right panel) at 300 GPa (6.67 Å^3 per atom). Though Fermi energy (E_F) has no physical meaning for a nonmetal, we set the highest valence band energy as E_F to indicate that, in analogy with the situation encountered with metals, all bands below E_F are occupied. **c**, Difference charge density (e Å^{-3}; crystal density minus superposition of isolated atomic densities) plotted in the (110) plane at 320 GPa (6.50 Å^3 per atom). **d**, Bandgaps calculated by DFT with the PAW potentials using VASP code (DFT_PAW, red diamonds) and the pseudopotential method using ABINIT code (DFT_PW, black squares), and the GW bandgap (GW, blue diamonds) as a function of volumes for Na-hP4. The upper axis represents theoretical pressure.

190 GPa (Fig. 2b). The position of the observed Raman peak and its dependence on pressure (Fig. 1b) agree well with theoretical calculations for Na-hP4, which possesses only one Raman-active E_{2g} mode. Enthalpy calculations (Fig. 3) confirm the stability of Na-hP4 beyond the tI19 phase. Note that the tI19→hP4 phase transition is predicted to occur at a pressure of 260 GPa (Fig. 3) yet is observed at pressures of ~200 GPa. This discrepancy may in part be due to the athermal nature of our calculations (that is, calculations at 0 K will neglect all entropic contributions), but we expect that the main reason is the well-known overstabilization of metallic states by density functional theory (DFT) calculations (see, for example, ref. 19).

Our calculations reveal that an insulating electronic state emerges because compression causes the 3*d* bands to rapidly drop in energy relative to the 3*p* bands and increasingly hybridize with them[4]. This hybridization is the key to strong electron localization: a marked charge accumulation occurs only in the open interstitial regions (Fig. 4c, Supplementary Figs 6 and 7). The shortest Na–Na distance in Na-hP4 is 1.89 Å at 300 GPa (6.67 Å^3 per atom), which implies strong core–valence overlap (the 3*s* and 2*p* orbital radii in Na are 1.71 and 0.28 Å, respectively) and even significant core–core overlap between neighbouring Na atoms (the ionic radius of Na^+ is 1.02 Å). A consideration of the geometry of charge maxima relative to the atoms implies *pd* and pd^2 hybridizations for Na1 in the octahedral sites and Na2 in the triangular prismatic coordination, respectively—consistent with the site-*l*-projected density of states (Fig. 4b and Supplementary Fig. 10). Thus, the insulating state in Na-hP4 arises from the strong localization of valence electrons in the interstices of Na-hP4 (Fig. 4c and Supplementary Fig. 6) enabled by *p*–*d* hybridization. In this context, it is interesting to note that in contrast to the *p*–*d* hybridization in Na, calculations[3] for other alkalis suggest they are dominated either by *p* electrons (Li) or by *d* electrons (K, Rb and Cs). Na-hP4 might thus be viewed as the intermediate structure between the six-coordinated structure predicted for Li and the ideal d.h.c.p. structures of K, Rb and Cs (ref. 3).

Note that while the stacking of close-packed layers of Na atoms is CACBCACB… (underlining indicates layers that contain interstitial electron density maxima; Fig. 4a) as in any d.h.c.p. structure, the interstitial charge density maxima are located only in layers A and B (that is, in every other layer) and form a nearly perfect h.c.p arrangement (layer stacking of ABAB… and $c/a \approx 1.3$–1.6, close to the ideal $c/a = 1.633$ for the h.c.p. structure). This finding explains the approximate halving of the c/a ratio as a reflection of the close packing of the interstitial electron density maxima, rather than Na atoms. This suggests that repulsion between the interstitial electron pairs is a major structure-forming interaction in Na-hP4.

As the number of ionic cores (each stripped of one valence electron) is exactly twice that of interstitial electron density maxima, Na-hP4 is an analogue of Ni_2In-type structures (considered also in ref. 7): the ionic cores form the Ni sublattice and the interstitial density maxima the In sublattice. And as pressure-induced transitions in the A_2X compounds[21] lead to an increase of the coordination number of X sites (that is, voids in Na-hP4), pressure-induced transitions in Na lead to an increase of the coordination number of lattice interstices: the coordination numbers are 8, 9 and 11, respectively, in the cI16, oP8 and hP4 phases of Na.

The case of dense Na provides an unexpectedly extreme example of a wide-gap insulator created by compression of a 'simple' metal. This novel dielectric consists of ionic cores and localized interstitial electron pairs, in analogy to electrides[22] where the interstitial electron density maxima play the role of anions. Dense insulating states such as reported here for Na may also be favoured in other elements and compounds when atomic cores are made to strongly overlap.

METHODS SUMMARY

For the experiments, sodium was loaded into a diamond-anvil cell in a nitrogen atmosphere and Raman spectra obtained with a 25 mW HeNe laser. X-ray studies were conducted at the Advanced Photon Source at the Argonne National Laboratory, USA. The evolutionary structure search used DFT for *ab initio* structure calculations.

Full Methods and any associated references are available in the online version of the paper at www.nature.com/nature.

Received 18 June 2008; accepted 19 January 2009.

1. Neaton, J. B. & Ashcroft, N. W. Pairing in dense lithium. *Nature* **400,** 141–144 (1999).
2. Tamblyn, I., Raty, J. Y. & Bonev, S. A. Tetrahedral clustering in molten lithium under pressure. *Phys. Rev. Lett.* **101,** 075703 (2008).
3. Ma, Y., Oganov, A. R. & Xie, Y. High pressure structures of lithium, potassium, rubidium predicted by ab initio evolutionary algorithm. *Phys. Rev. B* **78,** 014102 (2008).
4. Neaton, J. B. & Ashcroft, N. W. On the constitution of sodium at higher densities. *Phys. Rev. Lett.* **86,** 2830–2833 (2001).
5. Raty, J. Y., Schwegler, E. & Bonev, S. A. Electronic and structural transitions in dense liquid sodium. *Nature* **449,** 448–451 (2007).
6. Hanfland, M., Syassen, K., Christensen, N. E. & Novikov, D. L. New high-pressure phases of lithium. *Nature* **408,** 174–178 (2000).
7. Hanfland, M., Syassen, K., Loa, L., Christensen, N. E. & Novikov, D. L. Na at megabar pressures. *Poster at 2002 High Pressure Gordon Conference* (2002).
8. Gregoryanz, E. *et al.* Structural diversity of sodium. *Science* **320,** 1054–1057 (2008).
9. Shimizu, K., Ishikawa, H., Takao, D., Yagi, T. & Amaya, K. Superconductivity in compressed lithium at 20 K. *Nature* **419,** 597–599 (2002).
10. Struzhkin, V. V., Eremets, M. I., Gan, W., Mao, H. K. & Hemley, R. J. Superconductivity in dense lithium. *Science* **298,** 1213–1215 (2002).
11. Deemyad, S. & Schilling, J. S. Superconducting phase diagram of Li metal in nearly hydrostatic pressures up to 67 GPa. *Phys. Rev. Lett.* **91,** 167001 (2003).
12. Hanfland, M., Loa, I. & Syassen, K. Sodium under pressure: bcc to fcc structural transition and pressure-volume relation to 100 GPa. *Phys. Rev. B* **65,** 184109 (2002).
13. Gregoryanz, E., Degtyareva, O., Somayazulu, M., Hemley, R. J. & Mao, H. K. Melting of dense sodium. *Phys. Rev. Lett.* **94,** 185502 (2005).
14. Christensen, N. E. & Novikov, D. L. High-pressure phases of the light alkali metals. *Solid State Commun.* **119,** 477–490 (2001).
15. McMahon, M. I. *et al.* Structure of sodium above 100 GPa by single-crystal x-ray diffraction. *Proc. Natl Acad. Sci. USA* **104,** 17297–17299 (2007).

16. Glass, C. W., Oganov, A. R. & Hansen, N. USPEX—Evolutionary crystal structure prediction. *Comput. Phys. Commun.* **175,** 713–720 (2006).
17. Oganov, A. R. & Glass, C. W. Crystal structure prediction using ab initio evolutionary techniques: Principles and applications. *J. Chem. Phys.* **124,** 244704 (2006).
18. Oganov, A. R., Glass, C. W. & Ono, S. High-pressure phases of $CaCO_3$: Crystal structure prediction and experiment. *Earth Planet. Sci. Lett.* **241,** 95–103 (2006).
19. Ma, Y., Oganov, A. R. & Glass, C. W. Structure of the metallic ζ-phase of oxygen and isosymmetric nature of the ε-ζ phase transition: Ab initio simulations. *Phys. Rev. B* **76,** 064101 (2007).
20. Shishkin, M. & Kresse, G. Self-consistent GW calculations for semiconductors and insulators. *Phys. Rev. B* **75,** 235102 (2007).
21. Leger, J. M. & Haines, J. Crystal chemistry of the AX_2 compounds under pressure. *Eur. J. Solid State Inorg. Chem.* **34,** 785–796 (1997).
22. Dye, J. L. Electrides: From 1D Heisenberg chains to 2D pseudo-metals. *Inorg. Chem.* **36,** 3816–3826 (1997).

Supplementary Information is linked to the online version of the paper at www.nature.com/nature.

Acknowledgements We thank the Swiss National Science Foundation (grants 200021-111847/1 and 200021-116219), CSCS and ETH Zurich for the use of supercomputers. Parts of the calculations were performed on the Skif supercomputer (Moscow State University, Russia) and at the Joint Supercomputer Centre of the Russian Academy of Sciences (Moscow). We acknowledge partial support from DFG (grants Er 539/1/2-1) and the China 973 Program (no. 2005CB724400). Part of the experimental work was performed at GeoSoilEnviroCARS (Sector 13), Advanced Photon Source (APS), Argonne National Laboratory.

Author Contributions Y.M. proposed the research and predicted the new structures. Y.M., Y.X. and A.R.O. did the calculations. M.E., I.T., S.M. and V.P. performed the experiments. Y.M., A.R.O. and M.E. contributed substantially to data interpretation and wrote the paper. A.L. wrote the latest version of the structure prediction code, and M.V. helped in data analysis. Y.M, M.E. and A.R.O contributed equally to this paper.

Author Information Reprints and permissions information is available at www.nature.com/reprints. Correspondence and requests for materials should be addressed to Y.M. (mym@jlu.edu.cn).

METHODS

High-pressure experiments. Our diamond-anvil cell (DAC) experiments used diamonds with 30–50 μm culet bevelled to 8–9° and gaskets of rhenium or tungsten, or of cubic BN (cBN) powder mixed with epoxy. Sodium of 99.95% purity (Alfa Aesar) was loaded in a glove box in an atmosphere of pure nitrogen containing <0.1 p.p.m. oxygen and water. Before loading, the DAC was kept at 130 °C in a vacuum for 20 h to remove traces of water and gases at the surface of the gasket, thereby excluding reaction of the clamped sodium with rhenium or cBN/epoxy gaskets. Pressure was measured mainly by the Raman shift of the high-frequency edge of the stressed diamonds[23], and was in good agreement with the pressure obtained from X-ray diffraction data for Re and cBN in checking experiments. We estimate the pressure error to be within 5 GPa at the highest pressures, and less at lower pressures. An extremely sharp Raman edge of the diamond anvil indicated an excellent hydrostaticity of Na up to the highest pressures. An HeNe laser of power 25 mW was used for excitation of Raman spectra. Angle dispersive X-ray diffraction studies were performed at station 13-IDD at the Advanced Photon Source, Argonne National Laboratory, USA ($\lambda = 0.3344$ Å).

Evolutionary structure search and energy calculations. The evolutionary structure search was performed using the USPEX code[16–18], and the underlying *ab initio* structure relaxations were performed using DFT within the generalized gradient approximation (GGA)[24] and the frozen-core all-electron projector-augmented wave (PAW)[25,26] method, as implemented in the VASP code[27]. The quasiparticle energies were calculated within the GW approximation, as implemented in the ABINIT code[28], in which self-energy corrections are added to the Kohn–Sham energies at the selected k points that characterize the DFT bandgap.

We treated the 2*s*, 2*p* and 3*s* electrons as valence in the PAW potential adapted from the VASP library and used the plane-wave kinetic energy cut-off of 910 eV, which gave excellent convergence of the total energies, energy differences and structural parameters. We used the Monkhorst–Pack k meshes of $16 \times 16 \times 16$, $12 \times 12 \times 12$, $19 \times 19 \times 13$, $16 \times 16 \times 12$, $12 \times 16 \times 12$, $6 \times 6 \times 6$ and $20 \times 20 \times 14$ for f.c.c., cI16, α-Ga, Cs-IV, oP8, tI19 and hP4, respectively, which gave excellent convergence of the total energies (within 1 meV per atom) in the enthalpy calculations. GW calculations for Na-hP4 were performed with 131 k points in the first Brillouin zone, and an energy cut-off of 20 Ry was chosen for calculation of the Coulomb matrix. In the calculation of the self-energy matrix, 18 occupied bands and 120 unoccupied bands were explicitly treated. With the choice of these parameters, the bandgaps were found to converge within 0.01 eV.

23. Eremets, M. I. Megabar high-pressure cells for Raman measurements. *J. Raman Spectrosc.* **34**, 515–518 (2003).
24. Perdew, J. P., Burke, K. & Ernzerhof, M. Generalized gradient approximation made simple. *Phys. Rev. Lett.* **77**, 3865–3868 (1996).
25. Blöchl, P. E. Projector augmented-wave method. *Phys. Rev. B* **50**, 17953–17979 (1994).
26. Kresse, G. & Joubert, D. From ultrasoft pseudopotentials to the projector augmented-wave method. *Phys. Rev. B* **59**, 1758–1775 (1999).
27. Kresse, G. & Furthmüller, J. Efficient iterative schemes for ab initio total-energy calculations using a plane-wave basis set. *Phys. Rev. B* **54**, 11169–11186 (1996).
28. Gonze, X. *et al*. First-principles computation of material properties: The ABINIT software project. *Comput. Mater. Sci.* 25, 478–492 (2002); ⟨http://www.abinit.org/⟩.